

## Upper ocean warming and sea ice reduction in the East Greenland Current from 2003 to 2019

Laura de Steur <sup>1</sup>✉, Hiroshi Sumata <sup>1</sup>, Dmitry V. Divine<sup>1</sup>, Mats A. Granskog <sup>1</sup> & Olga Pavlova<sup>1</sup>

The sea ice extent and sea ice thickness in the Arctic Ocean have declined consistently in the last decades. The loss of sea ice as well as warmer inflowing Atlantic Water have major consequences for the Arctic Ocean heat content and the watermasses flowing out from the Arctic. Sustained observations from ocean moorings show that the upper ocean temperature across the Arctic outflow with the East Greenland Current in the Fram Strait has increased significantly between 2003 and 2019. Polar Water contains more heat in summer due to lower sea ice concentration and longer periods of open water upstream. Warm returning Atlantic Water has a greater presence in the central Fram Strait in winter since 2015, impacting winter sea ice thickness and extent. Combined, these processes result in a reduced sea ice cover downstream along the whole east coast of Greenland with inevitable consequences for winter-time ocean convection and ecosystem functioning.

<sup>1</sup>Norwegian Polar Institute, Tromsø, Norway. ✉email: [Laura.de.Steur@npolar.no](mailto:Laura.de.Steur@npolar.no)

The East Greenland Current (EGC) in the western Fram Strait transports sea ice and relatively fresh and cold Polar Water (PW, temperature  $< 0^{\circ}\text{C}$ ) from the central Arctic Ocean to the Nordic Seas and Subpolar North Atlantic<sup>1</sup> (Fig. 1). Alongside the southward flowing sea ice and PW, returning Atlantic Water (AW, temperature  $> 0^{\circ}\text{C}$ ) which gets cooled along its pathway, the EGC conveys both buoyant as well as dense components that feed the meridional overturning circulation (MOC) which is responsible for the mild climate in western Europe<sup>2–5</sup>. Sea ice export with the EGC through the Fram Strait has declined in the last decade primarily due to sea ice thinning<sup>6</sup> and reached a minimum in 2018, when both ice thickness and ice velocity were record low<sup>7</sup>. Besides reduced thickness of the ice exported from the Arctic Ocean, either by thinning upstream or nearby Fram Strait<sup>8</sup>, warming of the Nordic Seas<sup>9,10</sup> is expected to further reduce the sea ice cover east of Greenland, implying this region will be more exposed to winter-time ventilation<sup>11,12</sup>.

During the satellite era since 1979, sea ice extent (SIE), sea ice concentration (SIC), and sea ice thickness (SIT) in the Arctic Ocean have declined rapidly<sup>13,14</sup>. Reduced sea ice cover has led to warming of the ocean's surface and enhanced heat fluxes from ocean to atmosphere resulting in surface-based Arctic amplification<sup>15</sup>. The effects on Arctic sea ice are not only limited to summer and are now also observed in spring and winter, with decadal SIE loss in winter  $-3.4\%$  per decade after 2000<sup>16,17</sup>. The ice-albedo feedback allows for increased surface ocean heating, leading to increased sea surface temperatures<sup>18</sup>, which leaves an imprint also in winter as a near-surface temperature maximum in the Canada Basin<sup>19,20</sup>, and has amounted to significant warming of the halocline in the interior Beaufort Gyre<sup>21</sup>. Besides increasing solar heat input to the Arctic Ocean<sup>22</sup>, the inflow of warm Atlantic Water is an important source of heat<sup>23,24</sup>. The Eurasian Basin has been increasingly subject to Atlantification<sup>25,26</sup> with a reduced stability of the halocline and significant shoaling of Atlantic Water demonstrated by 15-year-long ocean mooring records in the eastern Arctic<sup>27</sup>. This weakening of the halocline allows for increased winter convection in that region and upward heat flux in the upper ocean, and contributes to reduced winter ice growth which, together with increased ice drift speeds<sup>8,28</sup>, can have an imprint on ice thickness in Fram Strait<sup>29</sup>.

The impact of the changes in the Arctic Ocean, in particular during the last decade, has become evident in the waters flowing from the Arctic through the Fram Strait as we will show here.

We present observed changes in upper ocean temperature, open water area, and ice thickness in both the southward flowing PW from the Arctic and returning AW in Fram Strait covering the period 2003 to 2019. Our results are from near-continuous data collected by two ocean moorings in the western Fram Strait (blue and red diamonds, respectively, in Fig. 1b and Fig. 2a, b). The temperature of PW on the shelf, which used to be characterized by a (weak) seasonal cycle related with melting and freezing<sup>30</sup>, is now marked by significant upper ocean warming in summer and can be related to increased open water and emerging (sub)surface temperature maxima. In addition, we show that a shift in presence of warm returning AW in the eastern EGC in winter occurred in mid 2015, which resulted in a significant reduction of the SIE in the northeastern Fram Strait in winter.

## Results

**Sea ice reduction in the Fram Strait.** Since 2015, significant changes have occurred in the SIE in the Fram Strait. Summer SIE in the EGC was greatly reduced in 2016, 2017, and 2018, relative to the long-term mean from August 2003–2015 (Fig. 2a). While the total Arctic SIE has its minimum in September, the largest reductions in the Fram Strait were already in August. Large northward retreat of the SIE up to  $79.8^{\circ}\text{N}$  in the EGC was observed in August 2017, and a much reduced eastward SIE and a vast open water area northwest of Svalbard was present in August 2018 (Fig. 2a). Also the winter SIE has been subject to significant changes (Fig. 2b). The largest negative anomalies to the winter sea ice climatology in the western Fram Strait were observed in January in recent years. In January 2016 and 2018, the sea ice edge at  $78.8^{\circ}\text{N}$  was 65 to 100 km further west (i.e., 3 to 5 degrees longitude) relative to the 2003–2015 average January SIE (Fig. 2b).

Open water fraction (OWF, see “Methods”) on the shelf (F14) shows periods of open water in summer during the whole record (Fig. 2c). The maximum OWF was large in summers 2017 and 2018 (Fig. 2c), as well as in 2004, 2006, and 2008. The duration of increased OWF, however, (i.e., defined here as the period with  $\text{OWF} > 0.5$ ) was  $\sim 10$  days longer in 2017, and consequently, the

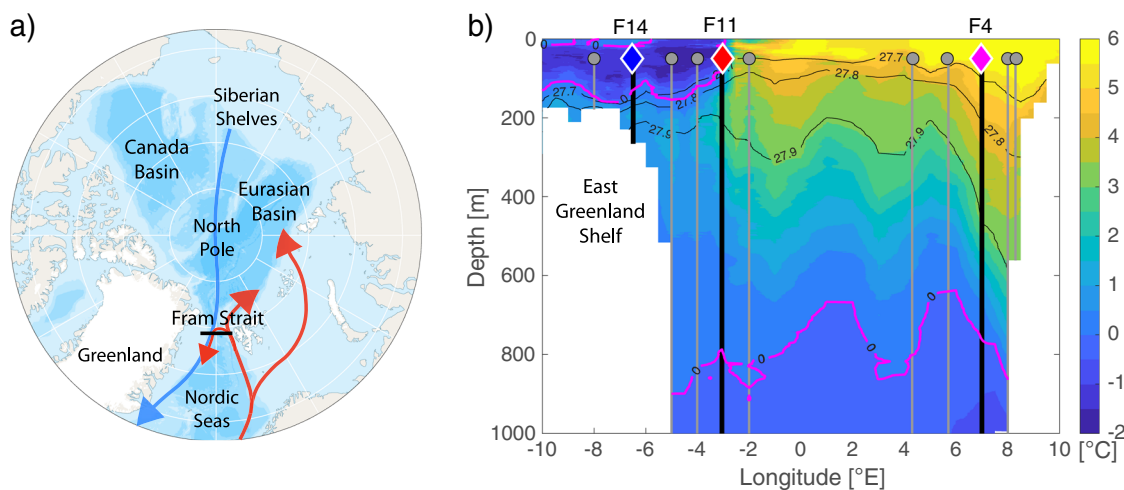


**Fig. 1** The study region: Fram Strait. **a** Map of the Arctic Ocean showing a schematic of the cold outflow of Polar Water from the Arctic to the East Greenland Current (blue arrow) and the warm inflow of Atlantic Water into the Arctic Ocean and its recirculation in Fram Strait (red arrows). The location of the section in the Fram Strait where the moorings are located at  $78^{\circ}50'\text{N}$  is marked with the horizontal black bar. **b** Vertical cross section of temperature in the Fram Strait at  $78^{\circ}50'\text{N}$  in September 2018 (obtained from shipboard hydrography) marking the locations of the moorings F14, F11, and F4 with thick vertical black lines and blue, red and magenta diamonds, respectively. The thin vertical gray lines mark other mooring sites in the strait (not used in this study). The background color is ocean temperature with  $0.5^{\circ}\text{C}$  intervals, the magenta lines mark the  $0^{\circ}\text{C}$  isotherm, and thin black contours mark the  $27.7$ ,  $27.8$ , and  $27.9\text{ kg m}^{-3}$  isopycnals.

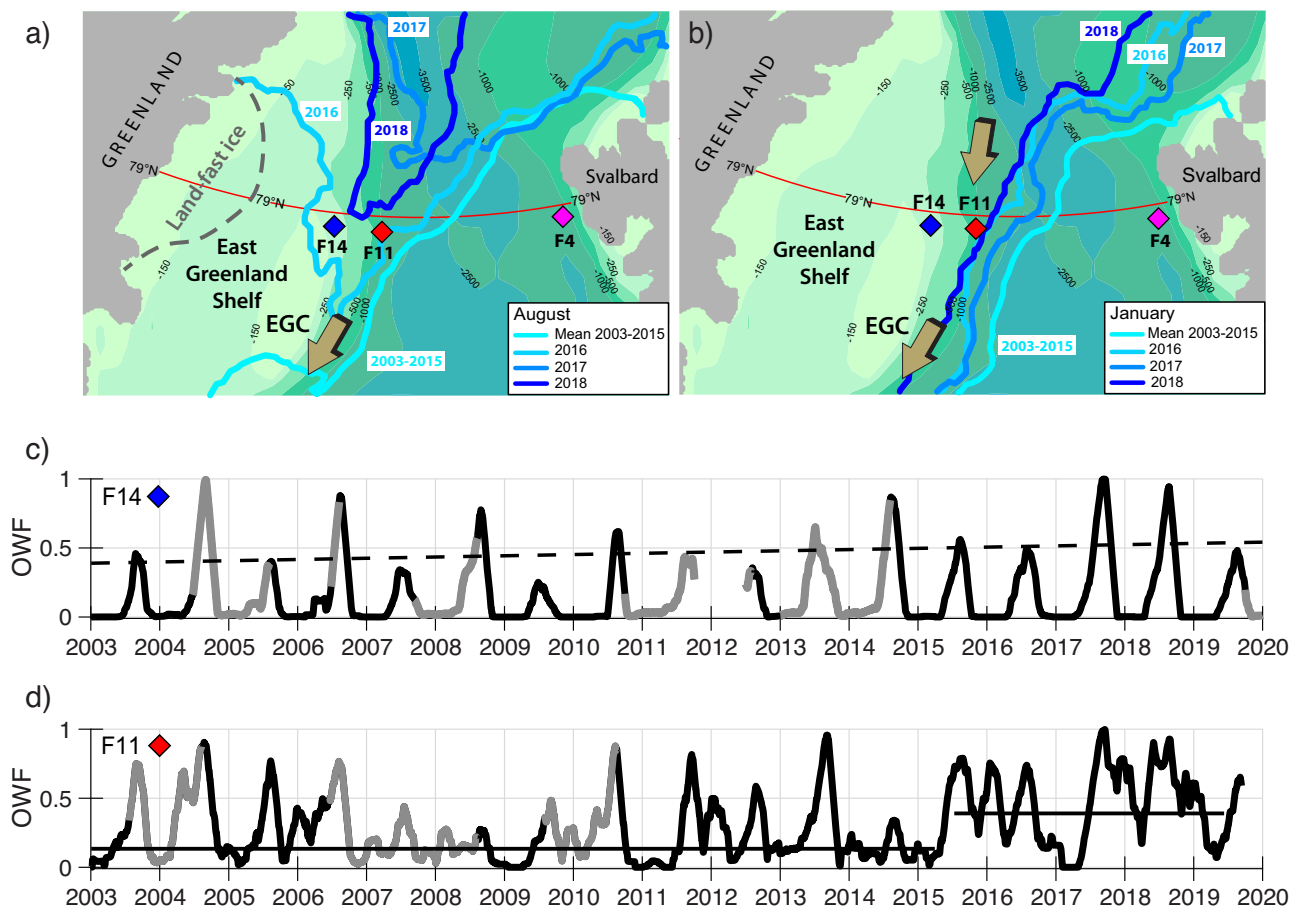


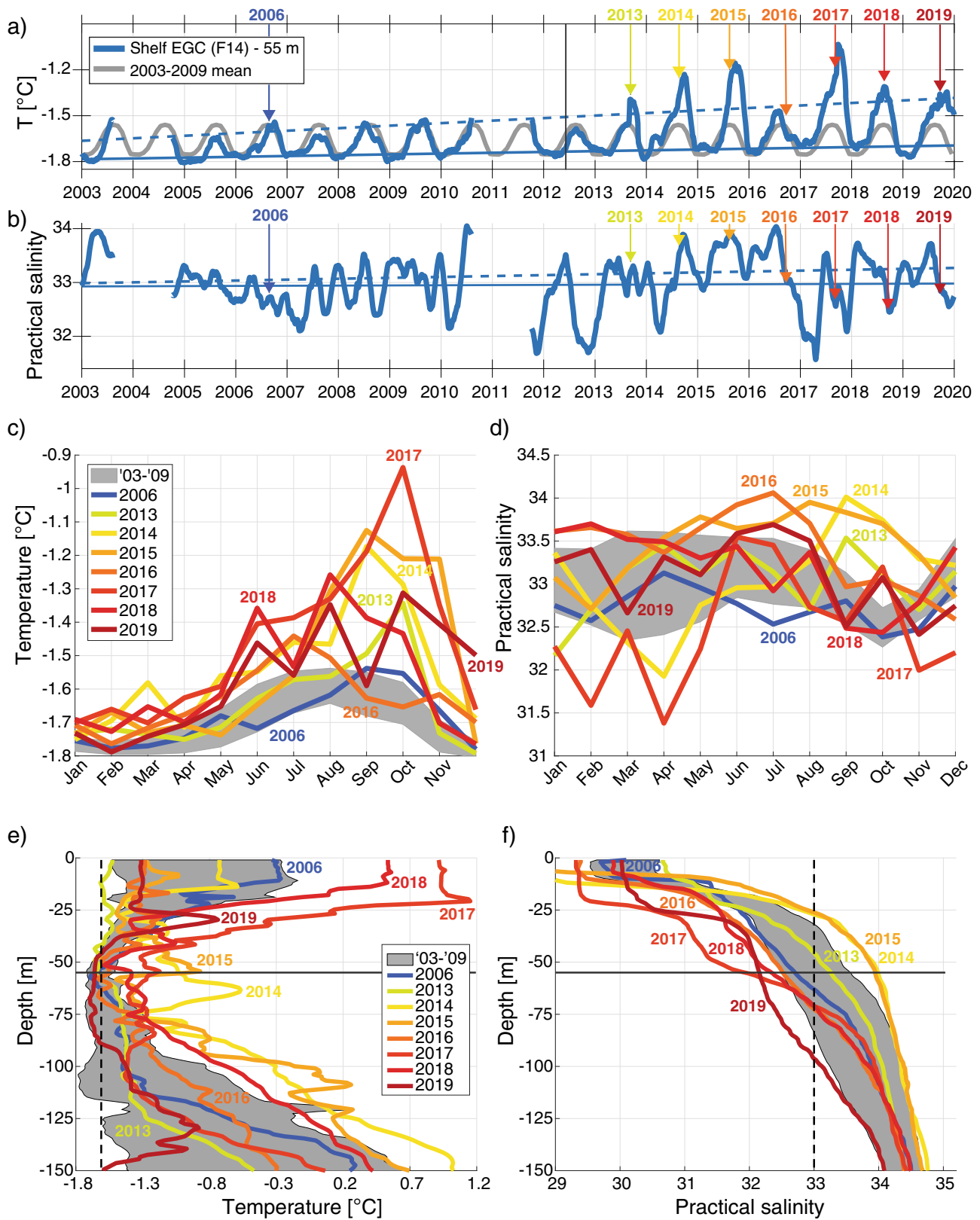
**Fig. 2** Sea ice extent (SIE) and open water fraction (OWF) in Fram Strait. SIE defined by 15% SIC in **a** August and **b** January as the mean for 2003–2015, and for individual years 2016, 2017, and 2018. The blue, red, and magenta diamonds mark mooring locations F14 (shelf), F11 (eastern EGC), and F4 (WSC), respectively. The background color shows bathymetry at intervals 150, 250, 500, 1000, 2500, and 3500 m. The brown arrows illustrate the flow direction of the EGC along the continental slope. OWF as a function of time at the **c** shelf mooring, and **d** eastern mooring where black marks in-situ data obtained from Upward Looking Sonar at the moorings, and gray indicates satellite derived values (AMSR-E/AMSR-2). The straight dashed black line in (**c**) is the linear summer (July–August–September) trend. The horizontal black lines in (**d**) indicate the winter (January–February–March) mean OWF pre-June 2015 and post-June 2015.

summer (JAS) trend of OWF is positive (Fig. 2c). OWF at the eastern mooring site (F11) also shows a seasonal cycle with maxima typically in summer up to 2015 (Fig. 2d). After 2015, however, the seasonality of OWF changed notably, and periods of open water increased significantly in winter (DJF) in 2016, 2018, and 2019. The long-term, winter-mean OWF of 0.15 before June 2015, increased to 0.49 after that time (Fig. 2d, black horizontal lines), while earlier, such large OWF at this site only occurred in summer.

**Polar Water temperature increase in summer.** Increasing summer temperatures are observed in the year-round ocean temperature record of PW at 55 m from mooring F14 on the shelf from January 2003 to December 2019 (Fig. 3a). Compared to the mean seasonal cycle before 2010, when little change occurred, the PW temperature at this depth shows a pronounced increase in seasonality manifested by increased temperatures in August–September and prolonged periods of higher temperatures lasting longer up until November, or even until December in 2019 (Fig. 3c). The resulting summer (JAS) temperature trend is 0.19 °C/decade while the winter-mean (JFM) temperature is much smaller but also positive at 0.07 °C/decade (Fig. 3a, Table S1). The associated salinity record of PW at this depth show a less distinct seasonal cycle, but shows a weak increasing trend in summer (Fig. 3b). There is no trend in winter salinity and the

evolution of salinity throughout the year compared to the mean seasonal cycle of 2003–2009 shows large interannual variability (Fig. 3d) demonstrating there is large variation in halocline waters transported southward on the shelf.

Surface and upper ocean temperature increases on the shelf in summer are further demonstrated by shipboard temperature and practical salinity profiles from late summer (Fig. 3e, f). There is large variability throughout the upper 150 m in recent years when PW temperature in summer exceeds the 2003–2009 summer (JAS) mean (Fig. 3e): 2017 and 2018 stand out in particular, with very high temperatures from ~50 m toward the surface; a subsurface temperature maximum is present between 25 and 75 m in 2014, 2015, and at about 30 m depth in 2019; in addition, temperatures below 75 m are warmer in 2014, 2015, and 2018. The associated practical salinity ( $S_p$ ) profiles also show a larger variation relative to the 2003–2009 mean JAS salinity (i.e.,  $S_p = 33$  at 55 m) from the shelf mooring (Fig. 3f). A clear division can be seen with practical salinity at 55 m being either fresher than  $S_p = 33$  (fresh upper halocline water) or saltier than  $S_p = 33$  (saline upper halocline water) (Fig. 3f). These profiles demonstrate that anomalously high temperatures toward the surface are related with a thicker layer of relatively fresh upper halocline water, while subsurface temperature maxima (at 55 m) are associated with saline halocline water at 55 m. Both origins, however, show higher temperatures since 2013.



The PW temperature evolution does not follow the temperature trend of the underlying AW, as shown by comparison with the core temperature of AW at a depth of 250 m on the shelf (Fig. S1a,b, Table S1). AW shows in fact a small negative trend in summer (JAS) of  $-0.07\text{ }^{\circ}\text{C}/\text{decade}$  related with anomalously warm AW in summers 2005 and 2006 and colder AW temperature during

summers 2017 and 2018. More importantly, temperature maxima in the AW layer do not coincide with the maxima in PW in 2014 and 2015, or 2017 (compare Fig. S1b with S1a). The winter (JFM) mean temperature trend, however, is still positive with  $0.18\text{ }^{\circ}\text{C}/\text{decade}$  and winter-mean AW temperatures at 250 m have not been below  $0.5\text{ }^{\circ}\text{C}$  since 2014 at this site.

**Fig. 3 Ocean properties on the Greenland shelf (mooring F14 at 6.5°W).** **a** Ocean temperature and **b** ocean salinity at a target depth of 55 m from the mooring. Dashed straight lines mark the linear trend in summer (July–August–September), solid straight lines mark the trend in winter (January–February–March). The gray line in **(a)** shows the mean seasonal cycle from 2003 to 2009. Seasonal cycle for **c** temperature, and **d** practical salinity at 55 m from the mooring. The gray shaded areas in **(c)** and **(d)** mark the mean  $\pm 1$  standard deviation from 2003 to 2009, colored lines show individual years when the summer ocean temperature at 55 m was larger than the 2003–2009 JAS mean. Vertical profiles of **e** temperature and **f** practical salinity from Aug/Sep on this site for the same years as in **(c, d)**. The gray shaded area marks the mean  $\pm 1$  std from 2003–2009, vertical dashed lines mark the 2003–2009 mean temperature and practical salinity at 55 m, respectively, horizontal solid lines mark 55 m depth (corresponding with the target depth from which panels **(a–d)** are shown).

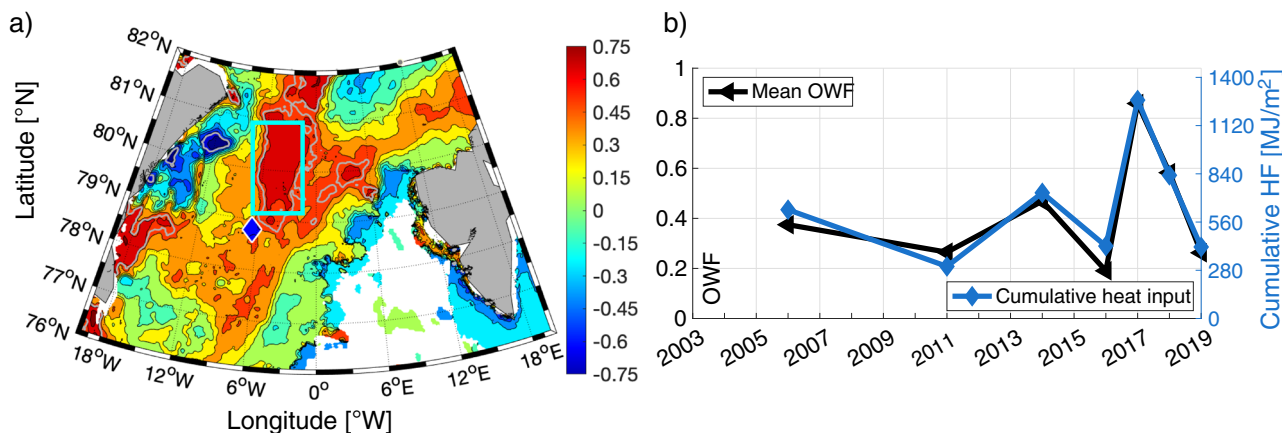


**Fig. 4 Relationship with summer-time open water fraction (OWF).** **a** Correlation map of monthly OWF anomaly with monthly ocean temperature anomaly at 55 m on the shelf (F14, blue diamond) where OWF leads by 1 month, for months when seasonal temperature anomaly was associated with monthly mean practical salinity  $S_p < 33$  at 55 m from the mooring. Thin gray contour mark the area with  $p$ -value  $< 0.05$ . The cyan box marks the upstream area for which OWF and heat input are calculated and shown in panel **(b)**. **b** Time series of mean OWF and cumulative mean heat flux in the area upstream of F14 during summer (July–August–September) for years when temperature was greater than the mean temperature between 2003–2009 and when practical salinity  $S_p < 33$  in summer.

The summer profiles indicate that increased temperature at 55 m depth in the PW can be differentiated into: (1) increased temperatures in the upper 50 m which is indicative of summer insolation of fresh halocline waters and have a practical salinity less than 33 at 55 m, or (2) appearance of warm and saline water masses related with AW derived watermasses with a practical salinity larger than 33 at 55 m. Correlations between the monthly mean ocean temperature anomaly at 55 m on the shelf (F14) with monthly OWF anomaly in the Fram Strait region are calculated for the summer months when the temperature anomaly was associated with monthly mean  $S_p$  at 55 m less than 33 (see Fig. 3e). Largest positive and significant correlations ( $R = 0.78$ ) are found with OWF in the area upstream and northeast of the shelf (Fig. 4a) with the ocean  $T$  at 6.5°W lagging the upstream OWF by 1 month. A 1-month lag is in agreement with an advection timescale of  $\sim 35$  days (using a mean observed upper ocean velocity of about  $5 \text{ cm s}^{-1}$  in summer<sup>31</sup>). The positive correlation of large temperature anomalies with OWF for the years with fresher halocline waters at 55 m depth, and smaller or no correlation in the years when the temperature anomaly was related with saline halocline waters (Fig. S3), demonstrates a clear link between reduced summer sea ice and increased heat input into the upper ocean upstream of the shelf mooring. Warm temperature anomalies at higher salinities are associated with subsurface temperatures originating from AW intrusions at about 50–75 m in the water column.

**Increased Atlantic Water presence in winter.** The year-round ocean temperature and salinity records from mooring F11 in the eastern EGC (Fig. 1b) shows distinct, but different changes over time than what has been observed on the shelf at F14 (Fig. 5a, b). The temperature record in the eastern EGC is typically marked by

intermittent occurrence of PW and AW as the PW/AW front moves east-west across this mooring site<sup>30</sup>. In June 2015, however, the intermittent regime changed to an AW dominated regime, as observed by a sudden increase of AW presence (from 0–20 to 20–30 days/month when  $T > 0^\circ\text{C}$  in winter, shown by orange diamonds in Fig. 5a, b). Until 2014, monthly mean temperatures stayed below  $0^\circ\text{C}$  except for summer (Fig. 5c, gray shade), while after 2015, positive temperatures are observed during all seasons pointing to a dissolution of the earlier seasonal cycle (Fig. 5c, orange-red lines). Salinity increases in winter-spring and larger interannual variation at this depth agree with the more frequent presence of AW after 2015 (Fig. 5d). The few available vertical hydrographic profiles at this site in spring demonstrate the change after 2015 (Fig. 5e, f). In 2018, the AW temperature maximum had shoaled up to  $\sim 75$  m (relative to 140–256 m for 2005–2008), and PW in the upper 55 m contained ten times more heat ( $3.1 \times 10^8 \text{ J m}^{-2}$  in 2018 vs a mean of  $3.0 \times 10^7 \text{ J m}^{-2}$  for 2005–2008) relative to the freezing point of seawater (based on the salinity from the respective hydrographic profiles). A shallow fresh layer in the top 20 m (Fig. 5e, red) indicates that the increased AW heat content in 2018 had likely caused local sea ice melt in spring.

Similar to PW, the temperature changes seen at 55 m depth in the eastern EGC do not correlate with temperature variations in the underlying AW at 250 m depth (Fig. S2, Table S1). However, a warm AW anomaly was present between 2015–2017, similar to 2005–2007. The AW temperature trend at 250 m in winter is positive at  $0.09^\circ\text{C}/\text{decade}$ , however, only half of the positive trend observed on the shelf, and is negative in summer with  $-0.05^\circ\text{C}/\text{decade}$ , similarly to that on the shelf (Table S1).

The increased presence of AW at shallow depths in the eastern EGC after 2015 is attributed to advection of warm AW from the

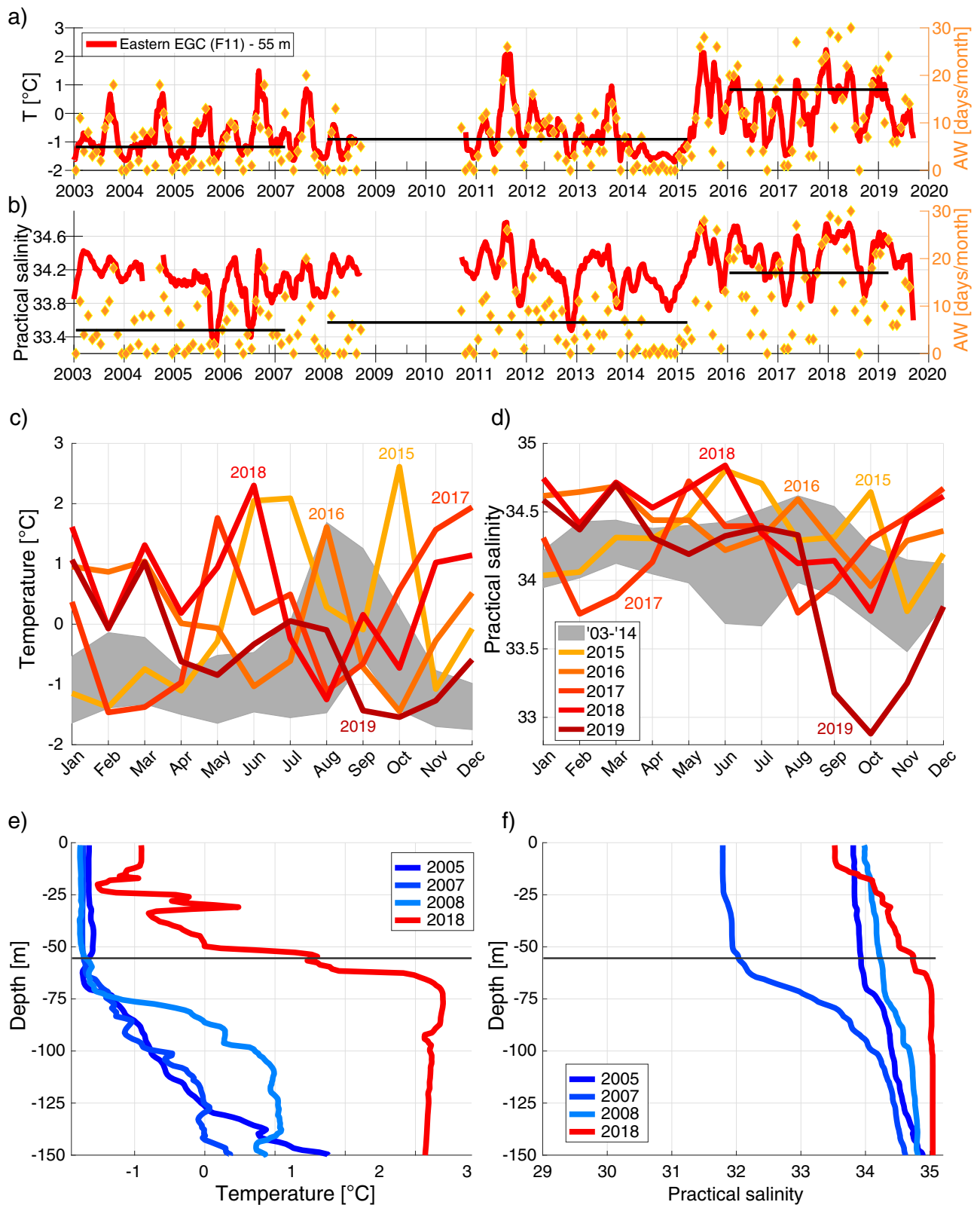


**Fig. 5** Ocean properties in the eastern EGC (mooring F11 at 3°W). **a** Ocean temperature and **b** ocean salinity at a target depth of 55 m from the mooring. Atlantic Water (AW) presence (defined as daily averaged temperature  $T > 0$  °C) is marked by orange diamonds (right axis). The horizontal black lines mark the mean AW presence during these periods. Seasonal cycles for **c** temperature, and **d** practical salinity at 55 m from the mooring. The gray shaded area marks the mean  $\pm 1$  standard deviation from 2003 to 2014 and the colored lines show individual years since 2015. Available vertical profiles of **e** temperature and **f** practical salinity from April/May at this site.

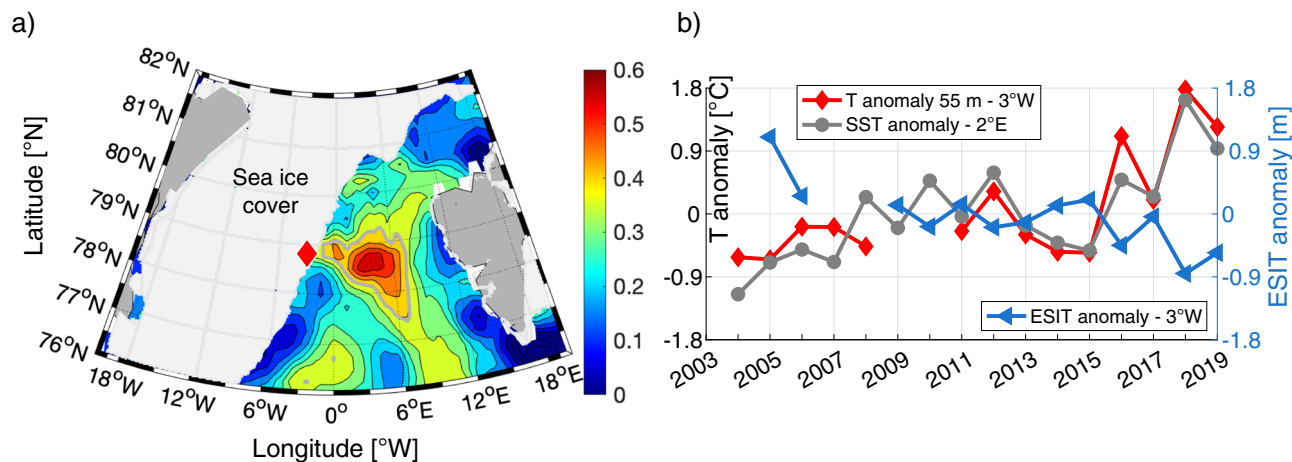


**Fig. 6 Relationship with winter-time sea-surface temperature (SST).** **a** Correlation map of monthly SST anomaly with monthly ocean temperature (T) anomaly at 55 m in the eastern EGC (F11, red diamond) where SST leads by 1 month, for months when the seasonal T anomaly at 55 m from the mooring exceeded 1 standard deviation. Thin gray contour east of F11 marks the area with  $p$ -value  $< 0.05$ . The light gray area west of F11 marks the sea ice cover covering the EGC and the Greenland shelf in January 2018. **b** Time series of SST anomaly at  $2^{\circ}\text{E}$ , T anomaly at 55 m from mooring F11, and Effective Sea Ice Thickness (ESIT) at the F11 site for extended winter periods (NDJFMA).

eastern or central Fram Strait. Monthly mean temperature at 55 m in the eastern EGC is strongly correlated with monthly sea surface temperature (SST) anomaly between  $1\text{--}4^{\circ}\text{E}$  at  $\sim 78.75^{\circ}\text{N}$  (Fig. 6a, Fig. S4). It particularly follows SST anomaly at  $2^{\circ}\text{E}$  closely for extended winter periods (NDJFMA) since 2011 (Fig. 6b,  $r = 0.89$ ). Observed ocean temperature anomaly from similar depths from mooring F4 in the West Spitsbergen Current (WSC) shows positive anomalies in subsurface temperature in 2016–2018 (Fig. S6e). However, these are smaller than the maximum observed anomalies at mooring F11 in the eastern EGC (Supp. Inf. Fig. S6c). All temperature records (eastern EGC, SST in central Fram Strait at  $\sim 2^{\circ}\text{E}$ , and WSC) were subject to a distinct regime shift in 2015, with the shift in the EGC a little delayed relative to that in the WSC (Fig. S6c, e, and “Methods”). Regional (Fram Strait) as well as large-scale (Nordic Seas) wind forcing, and turbulent heat flux in the Fram Strait, did not point to a shift occurring in 2015. The upper ocean volume transport of the EGC averaged over the upper 150 m, showed a reduction during the same time, which was associated with a reduced freshwater transport as of 2015<sup>32</sup>. This change is formally detected as a shift in southward velocity in the second half of 2015 (Figure S6b). We conclude that the shift in AW presence in the EGC was caused by advection of a warm AW anomaly from the Nordic Seas, with its largest expression in the central Fram Strait, and at nearly the same time, a reduction of the strength of the EGC.

**Impact on local and downstream sea ice concentration.** The observed temperature changes in the Fram Strait both on the shelf in summer as well as in the eastern EGC in winter leave significant imprints in the sea ice cover. Larger summer OWF upstream of F14 allows for more solar heating, followed by an increase in upper ocean temperature at 55 m at  $6.5^{\circ}\text{W}$ , and up to a  $2^{\circ}\text{C}$  positive SST anomaly in summer 2017 (Fig. 3e). For the years when anomalously high ocean temperature was associated with fresh halocline waters at 55 m, and when the correlation of temperature at 55 m with OWF was large, the cumulative heat input into the ocean into the upstream region (cyan box in Fig. 4a) in summer (JAS) is calculated (Fig. 4b, and “Methods”). The cumulative summer heat input amounted to a record high of  $\sim 1270 \text{ MJ/m}^2$  in 2017, and to  $830 \text{ MJ/m}^2$  in 2018, and which is 2.5 and 1.5 times the mean of  $520 \text{ MJ/m}^2$  before that time, respectively. This excess heat can consequently melt sea ice that is

transported from the north with the EGC. Alternatively, it can delay local ice growth. A simple 1D mixing model initialized with the hydrographic temperature profiles from the shelf and forced with daily ERA5 SST from September to December, shows that the anomalously warm ocean temperature in 2017 and 2018 could have delayed freezing of the ocean by 41 days and 13 days, respectively (relative to the 2003–2016 mean of  $13 \pm 8$  days after September 1st, Fig. S5). The fact that the large upstream open water area in 2017 and 2018 and the associated large increase in upper ocean temperature delayed the freeze up after September 1st significantly, demonstrates that the increased OWF also had an impact well after the summer season.

The increased presence of AW in the eastern EGC and large SST anomaly in the central Fram Strait in extended winter (NDJFMA), was strongly anti-correlated with the effective sea ice thickness (ESIT, see “Methods”) at  $3^{\circ}\text{W}$  (Fig. 6b). Winter ESIT shows about 0.5-m reduction from 1.3 m between 2009–2014 to 0.8 m in 2015–2018, and had an absolute minimum in winter 2018<sup>7</sup> which coincided with maximum ocean temperatures (Fig. 6b). A formal shift detection demonstrates that also ESIT as well as OWF were subject to a shift in mid-2015 (Fig. S6a), in agreement with the shifts found for ocean temperature at  $3^{\circ}\text{W}$  and SST at  $2^{\circ}\text{E}$ . In addition, the correlation between winter ESIT at the eastern ice edge of the EGC with ocean temperature at  $3^{\circ}\text{W}$  in winter increased from 0.65 to 1 since June 2015. We therefore suggest that with a general thinning of sea ice that arrives from the Arctic, the impact of warm returning AW on the sea ice cover in the Fram Strait has increased.

The effect of the observed ocean temperature changes in the Fram Strait, i.e., increases in the PW in summer and in the AW presence in winter, is found to propagate downstream and to have a significant imprint on the SIC along the eastern coast of Greenland in both seasons. Correlation maps of SIC downstream of the Fram Strait with ocean temperature at 55 m on the shelf in August show a significant correlation for several months lag (Fig. 7). This effect is detectable as far south as  $70^{\circ}\text{N}$  four months later, i.e., in December, demonstrating the downstream impact of the summer anomaly in Fram Strait (Fig. 7). Similarly, SIC downstream in the EGC correlates with ocean temperature at 55 m in the eastern EGC in December up to several months lag and is visible at 4 months lag, i.e., in April, as far south as  $67^{\circ}\text{N}$  (Fig. 8). The associated time series for selected sites downstream at given lags relative to the observed

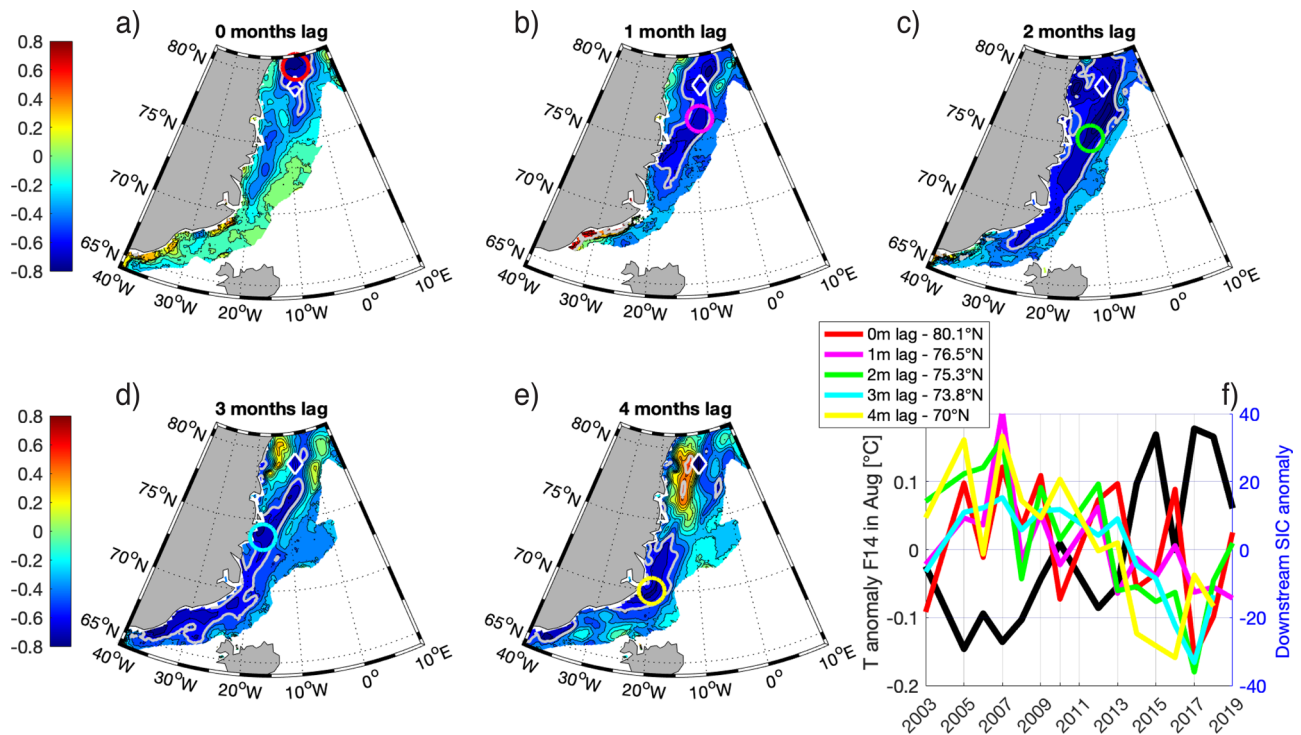


**Fig. 7** Correlation maps of sea ice concentration (SIC) in summer months with ocean temperature anomaly at 55 m on the shelf (F14, blue diamond). SIC for **a** 0 month, **b** 1 month, **c** 2 months, **d** 3 months, and **e** 4 months lag relative to ocean temperature in August, and **f** the associated time series at selected sites downstream. The colored circles in the correlation maps indicate the locations of which the time series are shown in the same color in **f**. Thin light gray contours mark the area with  $p$ -value < 0.05.

temperature changes in the Fram Strait demonstrates that the resultant SIC anomalies downstream in the EGC could be as much as 30% SIC (Figs. 7f and 8f). Our results show that the increased ocean temperatures in Fram Strait have a significant impact on the downstream evolution of sea ice in the EGC as far south as Denmark Strait.

We have shown that the summer temperature of the PW on the shelf has increased significantly over time, and became particularly high associated with large reductions in SIC in 2017 and 2018. In parallel, an increase of AW presence occurred on the eastern flank of the EGC, which resulted in a westward move of the sea ice edge in the Fram Strait in winter and caused enhanced thinning of sea ice with minimum thickness in 2018. The observed changes have significant impacts on ocean and sea ice in terms of seasonality, both locally as well as downstream. Our results are in agreement with observed SIT anomalies of up to 1 m along the EGC from 65°N to 80°N in April 2018<sup>17</sup> and we suggest a relationship with the increased ocean warming in (late) summer 2017 and 2018 in this region as well as the increased presence of AW in the central Fram Strait since 2015. The fact that the largest observed reduction in SIT in Fram Strait in 2018 did not originate from SIT changes in the central Arctic, but by a sudden reduction of SIT in the area just north of Fram Strait<sup>7</sup> provides additional evidence for the importance of regional processes nearby Fram Strait.

Recent studies have shown that changes in sea ice cover in the EGC has a significant impact on watermass modification and heat fluxes from the ocean to atmosphere east of Greenland<sup>11,12,34</sup>. Sea ice retreat allows the upper ocean to be more exposed to cooling by the atmosphere in winter, and hence areas of dense water formation could move further west towards Greenland with a potential increasing role for the EGC in delivering dense water to the MOC. Given present climate change and continued reduction in the Arctic sea ice cover, warming of PW will continue, and together with increased AW presence in the Fram Strait, will have a bigger impact

on the, now, much thinner sea ice exported from the Arctic<sup>8</sup>, and will contribute further to the reduction of the sea ice cover and changing the watermass characteristics along the whole coast of Greenland. In addition, changes in the vertical distribution of shelf water properties along eastern Greenland weaken the stratification, allowing for increased accessibility of nutrients in the surface waters, supporting increase in phytoplankton communities<sup>35</sup>. Disappearance of sea ice and ocean warming has already had significant implications for the marine ecosystems along the southeast coast of Greenland<sup>36</sup>, and one can infer that these conditions will propagate further north with the retreat of sea ice.

## Methods

**Data.** Temperature, salinity and pressure data are obtained from SBE37-SM MicroCATs (Sea-Bird Scientific) deployed on two ocean moorings in the Fram Strait Arctic Outflow Observatory at a latitude of 78°50'N between September 2002 and September 2019<sup>33</sup>. The western mooring (F14) is located on the shelf at a target longitude of ~6°30'W at a water depth of 270 m. The eastern mooring (F11) is located at a target longitude of ~3°04'W at a water depth of ~2440 m. The SBE37-SM were installed at two target depths on both moorings: 55 m and 250 m. Sampling interval of the SBE37-SM was 15 min. Data were quality controlled, despiked, and averaged into daily means. The running-mean time series shown in Figs. 1, 2, 3, and 5 were obtained applying a  $2N + 1$  running mean of the daily averaged data with  $N = 30$  days. Temperature data from SBE37-SM MicroCATs from approximately 60–80 m depth from mooring F4 at ~7°E in the WSC in eastern Fram Strait<sup>37</sup> (maintained by the Alfred Wegener Institute for Polar and Marine Research) were used to compare the temporal temperature evolution of the AW and identify possible regime shifts in the WSC.

The summer hydrographic profiles were obtained with a ship-based conductivity–temperature–depth (CTD) SBE911+ system<sup>38–44</sup>. Spring CTD profiles from 2005<sup>38</sup> and 2018<sup>45</sup> were obtained with a CTD SBE911+ system from the research vessel. Spring profiles from 2007 and 2008 were obtained with a CTD SBE19plus deployed from an ice floe<sup>33,46</sup>. Downcast profile data were averaged into 1 db vertical bins.

Measurements of sea ice draft from upward looking sonar (ULS)<sup>7</sup> from the shelf mooring F14 and eastern mooring F11 were used to calculate the OWF. OWF is equivalent to  $1 - \text{SIC}/100\%$ . Daily OWF time series were calculated directly from the raw sea ice draft data as cumulative fractions of observations flagged as open



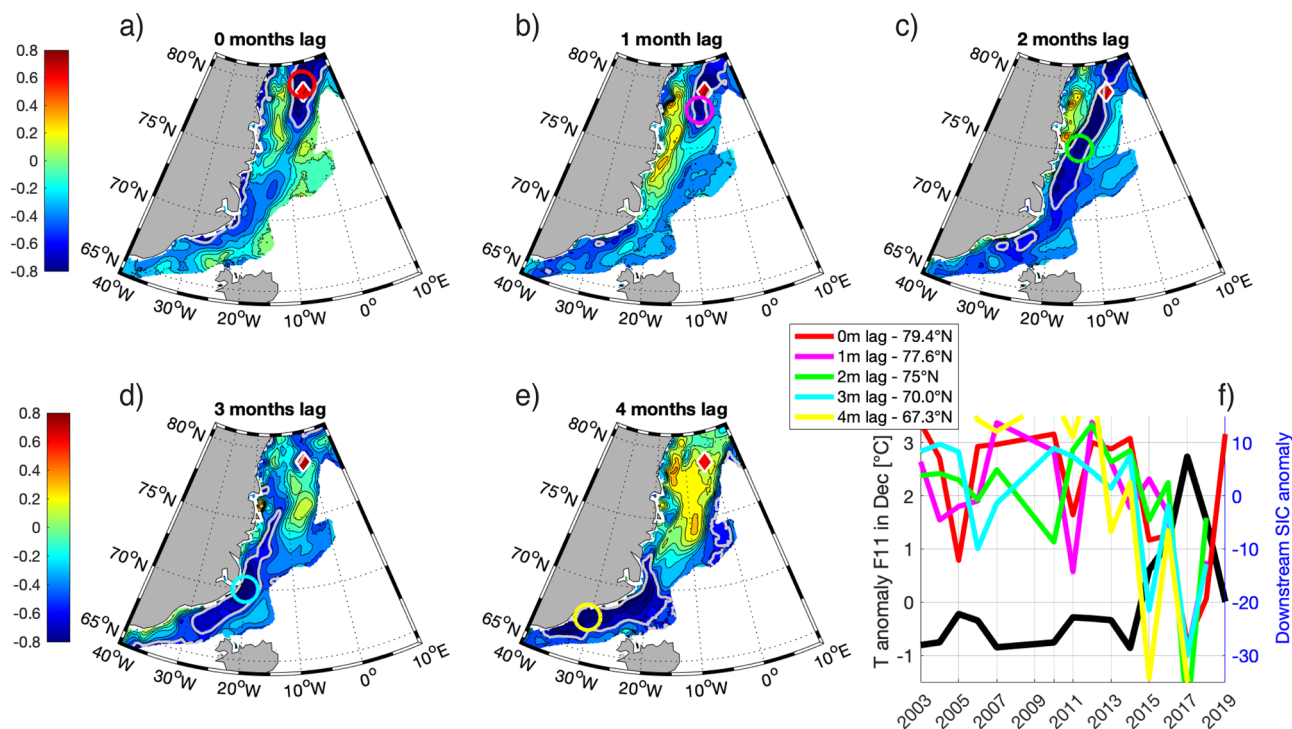


**Fig. 8** Correlation maps of sea ice concentration (SIC) in winter months with ocean temperature anomaly at 55 m in the eastern EGC (F11, red diamond). SIC for **a** 0 month, **b** 1 month, **c** 2 months, **d** 3 months, and **e** 4 months lag relative to ocean temperature in December, and **f** the associated time series at selected sites downstream. The colored circles in the correlation maps indicate the locations of which the time series are shown in the same color in **f**. Thin light gray contours mark the area with  $p$ -value < 0.05.

water, ice thinner than 5 cm and observations affected by waves. Poor quality observations were not included into the scheme. Effective sea ice thickness (ESIT) at the eastern mooring site F11 was obtained from averaging ice draft data from the ULS taking the OWF into account, i.e.,  $ESIT = SIT \times SIC$ .

Gaps in OWF from IPS data were filled with daily means from AMSR-E/2<sup>47</sup> data from the grid point closest to the mooring site (~1.1 to 1.6 km from the mooring site). AMSR-E/2 was also used to obtain OWF in the wider Fram Strait region to calculate heat input into the ocean upstream of the moorings (see details below). Sea ice concentration data for the calculation of ESIT was obtained from the Global Sea Ice Concentration Climate Data Records of the EUMETSAT OSI SAF<sup>48</sup>. Sea ice concentration data used in Fig. 2 were obtained from SSMR and SSM/I-SSMIS<sup>49</sup>.

ERA-5 reanalysis data was used to obtain daily mean surface shortwave downward flux (ssrd), as well as monthly mean SST and monthly mean 10-m winds<sup>50</sup>. Cumulative ocean heat input in the upstream area bounded by 79°N–80.9°N, 6.5°W–2°W (cyan box in Fig. 4a) for summer (JAS) was calculated by summing the daily mean heat input into the upstream ocean area taking into account the OWF, as follows:  $\sum OWF_{upstream} \cdot ssrd_{upstream} \cdot (1 - \alpha_0)$  with  $\alpha_0 = 0.07$ , the albedo of the ocean surface.

A 1-D model of ocean convection<sup>51</sup> was used to estimate when the ocean surface starts to freeze in autumn by applying atmospheric cooling. Vertical 1-m bin averaged conductivity–temperature–depth profiles of temperature and salinity collected each late August/early September at the mooring site F14 were used as the initial profile, and the model was forced with daily surface temperature from ERA-5 reanalysis from September 1st and run up to the end of December for each year. The number of days after September 1st when the temperature profile in the convective model was cooled down and mixed through sufficiently for the surface to start freezing was recorded for each year (Figure S5).

**Regime shift detection.** A sequential algorithm for regime shift detection<sup>52</sup> was applied to the daily time series of ocean temperature at 55 m and the time series of OWF and ESIT at the eastern EGC mooring site F11. It was also applied to the monthly mean ocean temperature anomaly (i.e., mean seasonal cycle removed) from the mooring F4 in the WSC at 7°E. This algorithm identifies discontinuities in a time series mean not requiring any a priori assumptions on the timing of the regime shifts. Testing for potential change points is conducted sequentially by checking if the anomaly of the data point is statistically significant from the mean value of the current regime. If it is found significant, following data points are sequentially used to assess the confidence of the shift, using regime shift index (RSI). RSI represents a cumulative sum of normalized deviations from the hypothetical mean level for the new regime, for which the difference from the mean level of current regime is statistically significant according to a Student's  $t$ -test. If RSI

remains positive for all points sequentially within the specified cut-off length, the null hypothesis of a constant mean is rejected. This allows one to conclude that a regime shift has occurred at that point in time<sup>53</sup>. We used a cut-off length of 5 years but other cut-off lengths (3, 4, and 6 years) were also tested. Due to a pronounced positive skewness of the original temperature time series, they were normalized using a quantile transform prior to application of the shift detection procedure. The quantile transform maps the cumulative density function (CDF) of the original series into a Gaussian CDF forcing the series to have a Gaussian probability density required by the shift detection method for the input data.

Before applying the shift detection method, short data gaps in the time series (i.e., 5 to 10 days when moorings were serviced) were linearly interpolated. The longest data gap in ocean temperature at the mooring in the eastern EGC mooring (F11) of nearly two years (from 2010 to 2012) was dealt with by selecting other periods of data in the time series to be used for filling in the gap. By doing this for 5 different choices of periods from other times in the time series, the sensitivity to the choice of the gap filling data segment could be tested. The tests confirmed that a shift occurred in 2015 and the result was found to be robust for all 5 cases with different choices to fill the 2-year data gap. Possible discontinuities arising at the start or end of the data segment that was used to fill the data gap had no impact on the result.

Regime shift tests were also carried out for monthly mean SST anomaly at 5 different longitudes at a latitude 78.75°N in the Fram Strait (Fig. S7) as well as for monthly anomalies (i.e., mean seasonal cycle removed) of turbulent heat flux, 10-m wind components, and wind stress curl over the Fram Strait, however, none of these parameters showed a regime shift.

## Data availability

The SBE37-SM MicroCAT temperature and salinity data from the moorings from the Fram Strait Arctic Outflow Observatory are available at <https://doi.org/10.21334/npolar.2019.8bb85388> and <https://doi.org/10.21334/npolar.2021.c4d80b64>. Mooring data from the AWI mooring F4 in the eastern Fram Strait can be found at <https://doi.org/10.1594/PANGAEA.900883> and <https://doi.org/10.1594/PANGAEA.905565>. Hydrographic temperature and salinity profiles from the summer cruises to the Fram Strait are available at <https://doi.org/10.21334/npolar.2014.e3d4f892>, <https://doi.org/10.21334/npolar.2022.493ea7ad>, <https://doi.org/10.21334/npolar.2022.52ecd98>, <https://doi.org/10.21334/npolar.2022.29c6e2c7>, <https://doi.org/10.21334/npolar.2022.44db5c55>, <https://doi.org/10.21334/npolar.2022.2c646c2e>, <https://doi.org/10.21334/npolar.2022.5066a075>. The hydrographic data from late winter and spring are available at <https://doi.org/10.21343/7jqb-5930> (KVS2007 cruise), <https://doi.org/10.21343/btym-vh89> (KVS2008 cruise), and [https://www.bodc.ac.uk/data/published\\_data\\_library/catalogue/10.5285/84988765-5fc2-5bba-e053-6c86abc05d53](https://www.bodc.ac.uk/data/published_data_library/catalogue/10.5285/84988765-5fc2-5bba-e053-6c86abc05d53) (JR17005 cruise 2018).

Received: 21 December 2022; Accepted: 26 June 2023;

Published online: 18 July 2023

## References

- Aagaard, K. & Coachman, L. K. The East Greenland current north of Denmark Strait: Part 1. *Arctic* **21**, 181–200 (1968).
- Mauritzen, C. Production of dense overflow waters feeding the North Atlantic across the Greenland-Scotland Ridge. *Deep Sea Res. Part I* **43**, 769–806 (1996).
- Eldevik, T. et al. Observed sources and variability of Nordic seas overflow. *Nat. Geosci.* **2**, 406–410 (2009).
- Le Bras, I. et al. How much Arctic fresh water participates in the subpolar overturning circulation? *J. Phys. Oceanogr.* **51**, 955–973 (2021).
- Stouffer, R. J., Co authors. Investigating the causes of the response of the thermohaline circulation to past and future climate changes. *J. Climate* **19**, 1365–1387 (2006).
- Spreen, G., de Steur, L., Divine, D. V., Gerland, S., Hansen, E. & Kwok, R. Arctic sea ice volume export through Fram Strait from 1992 to 2014. *J. Geophys. Res. Oceans* **125**, e2019JC016039 (2020).
- Sumata, H., de Steur, L., Gerland, S., Divine, D. V. & Pavlova, O. Unprecedented decline of Arctic sea ice outflow in 2018. *Nat. Commun.* **13**, 1747 (2022).
- Sumata, H., de Steur, L., Divine, D. V., Granskog, M. A. & Gerland, S. Regime shift in Arctic Ocean sea ice thickness. *Nature* **615**, 443–449 (2023).
- Mork, K. A., Skagseth, Ø. & Soiland, H. Recent warming and freshening of the Norwegian Sea observed by Argo data. *J. Climate* **32**, 3695–3705 (2019).
- Tsubouchi, T. et al. Increased ocean heat transport into the Nordic Seas and Arctic Ocean over the period 1993–2016. *Nat. Clim. Chang.* **11**, 21–26 (2021).
- Våge, K. et al. Ocean convection linked to the recent ice edge retreat along east Greenland. *Nat. Commun.* **9**, 1287 (2018).
- Moore, G. W. K. et al. Sea-ice retreat suggests re-organization of water mass transformation in the Nordic and Barents Seas. *Nat. Commun.* **13**, 67 (2022).
- Parkinson, C. L. & Cavalieri, D. J. Antarctic sea ice variability and trends, 1979–2010. *Cryosphere* **6**, 871–880 (2012).
- Lindsay, R. & Schweiger, A. Arctic sea ice thickness loss determined using subsurface, aircraft, and satellite observations. *Cryosphere* **9**, 269–283 (2015).
- Serreze, M. C., Barrett, A. P., Stroeve, J. C., Kindig, D. N. & Holland, M. M. The emergence of surface-based Arctic amplification. *Cryosphere* **3**, 11–19 (2009).
- Stroeve, J. & Notz, D. Changing state of Arctic sea ice across all seasons. *Environ. Res. Lett.* **13**, 103001 (2018).
- Perovich, D. et al. Sea ice. in *Arctic Report Card 2019* (eds. Richter-Menge, J., Druckenmiller, M. L. & Jeffries, M.) <http://www.arctic.noaa.gov/Report-Card> (2019).
- Perovich, D. K., Light, B., Eicken, H., Jones, K. F., Runciman, K. & Nghiem, S. V. Increasing solar heating of the Arctic Ocean and adjacent seas, 1979–2005: Attribution and role in the ice-albedo feedback. *Geophys. Res. Lett.* **34**, L19505 (2007).
- Jackson, J. M., Carmack, E. C., McLaughlin, F. A., Allen, S. E. & Ingram, R. G. Identification, characterization, and change of the near-surface temperature maximum in the Canada Basin, 1993–2008. *J. Geophys. Res.* **115**, C05021 (2010).
- Timmermans, M.-L. The impact of stored solar heat on Arctic sea ice growth. *Geophys. Res. Lett.* **42**, 6399–6406 (2015).
- Timmermans, M.-L., Toole, J. & Krishfield, R. Warming of the interior Arctic Ocean linked to sea ice losses at the basin margins. *Sci. Adv.* **4**, eaat6773 (2018).
- Nicolaus, M., Katlein, C., Maslanik, J. & Hendricks, S. Changes in Arctic sea ice result in increasing light transmittance and absorption. *Geophys. Res. Lett.* **39**, L24501 (2012).
- Rudels, B., Jones, E. P., Anderson, L. G. & Kattner, G. in *The Role of the Polar Oceans in Shaping the Global Climate* (eds. Johannessen, O. M., Muench, R. D. & Overland, J. E.), 33–46 (American Geophysical Union, 1994).
- Quadfasel, D., Sy, A., Wells, D. & Tunik, A. Warming in the Arctic. *Nature* **350**, 385 (1991).
- Årthun, M., Eldevik, T., Smedsrud, L. H., Skagseth, Ø. & Ingvaldsen, R. B. Quantifying the Influence of Atlantic Heat on Barents Sea Ice Variability and Retreat. *J. Climate* **25**, 4736–4743 (2012).
- Polyakov, I. V. et al. Greater role for Atlantic inflows on sea-ice loss in the Eurasian Basin of the Arctic Ocean. *Science* <https://doi.org/10.1126/science.aai8204> (2017).
- Polyakov, I. V. et al. Weakening of cold halocline layer exposes sea ice to oceanic heat in the eastern Arctic Ocean. *J. Climate* **33**, 8107–8123 (2020).
- Kwok, R., Spreen, G. & Pang, S. Arctic sea ice circulation and drift speed: decadal trends and ocean currents. *J. Geophys. Res.* **118**, 1–18 (2013).
- Belter, H. et al. Interannual variability in Transpolar Drift summer sea ice thickness and potential impact of Atlantification. *Cryosphere* **15**, 2575–2591 (2021).
- Holfort, J. & Hansen, E. Timeseries of Polar Water properties in Fram Strait. *Geophys. Res. Lett.* **32**, L19601 (2005).
- De Steur, L., Hansen, E., Mauritzen, C., Beszczynska-Möller, A. & Fahrbach, E. Impact of recirculation on the East Greenland Current in Fram Strait: results from moored current meter measurements between 1997 and 2009. *Deep Sea Res. Part I* **92**, 26–40 (2014).
- Karpouzoglou, T., de Steur, L., Smedsrud, L. H. & Sumata, H. Observed changes in the Arctic freshwater outflow in Fram Strait. *J. Geophys. Res. Oceans* **127**, e2021JC018122 (2022).
- Hansen, E. & Dodd, P. A. *Data Collected during the KV Svalbard Cruise in 2007*. <https://doi.org/10.21343/7jqb-5930> (Norwegian Meteorological Institute, 2011).
- Renfrew, I. A. et al. The Iceland Greenland Seas Project. *BAMS* **100**, 1795 (2019).
- Gjelstrup, C. V. B. et al. Vertical redistribution of principle water masses on the Northeast Greenland Shelf. *Nat. Commun.* **13**, 7660 (2022).
- Heide-Jørgensen, M. P. et al. A regime shift in the Southeast Greenland marine ecosystem. *Global Change Biol.* **29**, 668–685 (2023).
- Appen, W.-Jv, Schauer, U., Hattermann, T. & Beszczynska-Möller, A. Seasonal cycle of mesoscale instability of the West Spitsbergen Current. *J. Phys. Oceanogr.* **46**, 1231 (2016).
- Norwegian Polar Institute. Physical oceanography data (1981 to 2015) [Data set]. Norwegian Polar Institute. <https://doi.org/10.21334/npolar.2014.e3d4f892> (2014).
- Dodd, P. A. et al. CTD profiles from NPI cruise FS2014 to the Fram Strait including auxiliary sensors. Norwegian Polar Institute. <https://doi.org/10.21334/npolar.2022.493ea7ad> (2022).
- Dodd, P. A. et al. CTD profiles from NPI cruise FS2015 to the Fram Strait including auxiliary sensors. Norwegian Polar Institute. <https://doi.org/10.21334/npolar.2022.52ecd98> (2022).
- Dodd, P. A. et al. CTD profiles from NPI cruise FS2016 to the Fram Strait including auxiliary sensors. Norwegian Polar Institute. <https://doi.org/10.21334/npolar.2022.29c6e2c7> (2022).
- Dodd, P. A. et al. CTD profiles from NPI cruise FS2017 to the Fram Strait including auxiliary sensors. Norwegian Polar Institute. <https://doi.org/10.21334/npolar.2022.44db5c55> (2022).
- Dodd, P. A. et al. CTD profiles from NPI cruise FS2018 to the Fram Strait including auxiliary sensors. Norwegian Polar Institute. <https://doi.org/10.21334/npolar.2022.2c646c2e> (2022).
- Dodd, P. A. et al. CTD profiles from NPI cruise FS2019 to the Fram Strait including auxiliary sensors. Norwegian Polar Institute. <https://doi.org/10.21334/npolar.2022.5066a075> (2022).
- Hopkins, J., Brennan, D., Abell, R., Sanders, R. W. & Mountfield, D. CTD data from NERC Changing Arctic Ocean Cruise JR17005 on the RRS James Clark Ross, May–June 2018 (version 2). British Oceanographic Data Centre, National Oceanography Centre, NERC, UK. <https://doi.org/10.5285/84988765-5fc2-5bba-e053-6c86abc05d53> (2019).
- Hansen, E. & Dodd, P. A. *Data Collected During the KV Svalbard Cruise in 2008*. <https://doi.org/10.21343/btym-vh89> (Norwegian Meteorological Institute, 2011).
- Spreen, G., Kaleschke, L. & Heygster, G. Sea ice remote sensing using AMSR-E 89GHz channels. *J. Geophys. Res.* **113**, C02S03 (2008).
- Laverge, T. et al. Version 2 of the EUMETSAT OSI SAF and ESA CCI sea-ice concentration climate data records. *Cryosphere* **13**, 49–78 (2019).
- Cavalieri, D. J., Parkinson, C. L., Gloersen, P. & Zwally, H. J. Sea Ice Concentrations from Nimbus-7 SMMR and DMSP SSM/I-SSMIS Passive Microwave Data, Version 1. Monthly Mean Gridded Ice Concentration Fields. Boulder, Colorado USA. NASA National Snow and Ice Data Center Distributed Active Archive Center. <https://doi.org/10.5067/8GQ8LZQVLOVL> (1996).
- Hersbach, H. et al. ERA5 monthly averaged data on single levels from 1959 to present. Copernicus Climate Change Service (C3S) Climate Data Store (CDS) (2019).
- Darelius, E., Nilsen, F., Smedsrud, L. H. & Årthun, M. *Ice Formation and Convection—A One Dimensional Model*. (Geophysical Institute, University of Bergen, 2021).
- Rodionov, S. N. A sequential algorithm for testing climate regime shifts. *Geophys. Res. Lett.* **31**, L09204 (2004).
- Rodionov, S. & Overland, J. E. Application of a sequential regime shift detection methods to the Bering Sea ecosystem. *ICES J. Mar. Sci.* **62**, 328–332 (2005).

## Acknowledgements

This study has been made possible through the long-term observations from the Fram Strait Arctic Outflow Observatory maintained by the Norwegian Polar Institute. This

work was supported by the Norwegian Research Council project FreshArc through the FRIPRO program (grant 286971). H.S. and M.A.G. acknowledge funding from the European Union's Horizon 2020 research and innovation program under grant no. 101003826 via project CRiceS (Climate Relevant interactions and feedbacks: the key role of sea ice and Snow in the polar and global climate system). We thank Paul. A. Dodd for coordinating and overseeing the shipboard hydrographic data collection. We thank Kristen Fossan for the dedicated work on servicing the moorings in the Fram Strait Arctic Outflow Observatory.

### Author contributions

L.d.S. led and carried out the observational analysis and wrote the original draft. All authors contributed to data collection. H.S., D.D., and O.P. derived and provided sea ice data products to the study. All authors contributed to interpretation of the results and review and editing of the paper. L.d.S. and M.A.G. acquired funding.

### Competing interests

The authors declare no competing interests.

### Additional information

**Supplementary information** The online version contains supplementary material available at <https://doi.org/10.1038/s43247-023-00913-3>.

**Correspondence** and requests for materials should be addressed to Laura de Steur.

**Peer review information** *Communications Earth & Environment* thanks Tom Haine and the other, anonymous, reviewer(s) for their contribution to the peer review of this work. Primary Handling Editors: Heike Langenberg. A peer review file is available.

**Reprints and permission information** is available at <http://www.nature.com/reprints>

**Publisher's note** Springer Nature remains neutral with regard to jurisdictional claims in published maps and institutional affiliations.



**Open Access** This article is licensed under a Creative Commons Attribution 4.0 International License, which permits use, sharing, adaptation, distribution and reproduction in any medium or format, as long as you give appropriate credit to the original author(s) and the source, provide a link to the Creative Commons licence, and indicate if changes were made. The images or other third party material in this article are included in the article's Creative Commons licence, unless indicated otherwise in a credit line to the material. If material is not included in the article's Creative Commons licence and your intended use is not permitted by statutory regulation or exceeds the permitted use, you will need to obtain permission directly from the copyright holder. To view a copy of this licence, visit <http://creativecommons.org/licenses/by/4.0/>.

© The Author(s) 2023